Self-Referenced Method for Geometrical Distortion Removal in THz Time-Domain Reflection Imaging

Alessia Artesani, Marina Ljubenović, Arianna Traviglia, and Stefano Bonetti

***Abstract*—In this article, we develop a method for removing the phase drift induced by physically distorted object in terahertz time-domain reflection imaging (THz-TDRI). The proposed approach is defined as self-referenced, as it does not rely on any numerical parameter optimization nor extra instrumental components, and it is based on the unique manipulation of time-domain imaging data. In fact, we demonstrate that the problem can be solved assuming a linear contribution of the temporal shift induced by surface curvature. We illustrate how the self-referenced method is modeled and implemented, and we report the results obtained on two objects with different characteristics: a tilted and highly reflective surface, and a warped and heterogeneous surface. The proposed method demonstrates how to successfully remove the phase alterations induced on the reflected electric field, and how to repair the heavily corrupted images in the frequency-domain.**

***Index Terms*—Image restoration, phase variation problem, reflection geometry, terahertz time-domain reflection imaging (THz-TDS).**

I. Introduction

THE use of electromagnetic radiation at terahertz frequencies (from 0.1 to 10 THz) is becoming highly popular, mostly thanks to the increased availability of stable devices. A valuable characteristic of THz radiation is that it can penetrate a wide range of nonconducting materials, including plastics, polymers, and ceramics [1], [2], [3]. It is strongly absorbed by polar molecules, such as water [4], reflected by metals [5], and at the same time, it is not ionizing and harmless for biological tissues [6]. For these reasons, THz-waves are broadly applicable in many disciplines, such as bio-medicine, agriculture, and security and communication services [7], [8], [9].

Terahertz time-domain spectroscopy (THz-TDS) is appreciated especially in the field of material studies because it enables to simultaneously extract the real and imaginary part of the refractive index from the far-field Fresnel-equations [10], [11]. This is because the technique is phase-sensitive and it does not only capture the intensity of the electric field $|E(t)|$, but also its time-dependent amplitude E(t) [1]. The adoption of THz-TDS in transmission setups is preferred in many applications because it provides more precisely the phase variation, uniquely determined by the sample optical properties in the far-infrared region and its physical thickness. However, when dealing with opaque objects that are too thick or have a high dielectric loss for allowing the measurement in transmission mode, the reflection geometry represents the only option. In this configuration, the phase measurement suffers of higher uncertainty, because of displacement in the relative positioning of reference and sample objects [12], [13]. This represents a major experimental constraint for THz reflection measurements.

In imaging modality, the limitations in phase accuracy are unavoidable if the object has surface tilting or warping (i.e., curvature, physical distortions, irremovable irregularity at the surface). In terahertz time-domain reflection imaging (THz-TDRI), the phase shift is induced by the combined-effect of dispersive properties of material and geometrical distortion of the object. Moreover, the magnitude of the time traces drops when the reflective surface deviates from the optimized focus position, while additional signal losses might occur due to optical misalignment between the reflected beam and the collecting parabolic mirror [13]. Because in time-domain spectroscopy the spatial and spectral dependencies are coupled [14], [15], the object distortion has the undesirable consequence of modifying both the amplitude and the phase of the reflected electric field in the frequency-domain. This is why the object tilting or warping intrinsically generates inaccuracy in the extraction of the complex index of refraction value.

Despite these inherent limitations, the reflection geometry turns out to be profitable for investigating multiple-layer systems and turbid media. For example, there are remarkable examples of studies that used THz-TDRS for analyzing cultural heritage objects, i.e., painting, ceramics, easel, and more [16], [17], [18], or for investigating tissues and organs in the biomedical fields [19], [20]. The presence of composite materials is quite common in these domains, and their identification is important for their specific goals, e.g., restoration treatments in the former examples [21], and the diffusion of tumors or disease diagnosis in the second cases [22], [23]. To date, optical coherence tomography (OCT) has been employed for obtaining cross-sectional images of the first layers of objects or biological tissues/membranes

Manuscript received 10 May 2022; revised 24 November 2022; accepted 13 December 2022. Date of publication 21 December 2022; date of current version 3 March 2023. *(Corresponding author: Alessia Artesani.)*

Alessia Artesani is with the Center for Cultural Heritage Technology, Istituto Italiano di Tecnologia, 30172 Venice, Italy, and also with the Department of Biomedical Sciences, Humanitas University, 20090 Milan, Italy (e-mail: alessia.artesani@hunimed.eu).

Marina Ljubenović and Arianna Traviglia are with the Center for Cultural Heritage Technology, Istituto Italiano di Tecnologia, 30172 Venice, Italy (e-mail: marina.ljubenovic@iit.it; arianna.traviglia@iit.it).

Stefano Bonetti is with the Department of Molecular Sciences and Nanosystems, Ca'Foscari University of Venice, 30172 Venice, Italy, and also with the Department of Physics, Stockholm University, 106 91 Stockholm, Sweden (e-mail: stefano.bonetti@unive.it).

Color versions of one or more figures in this article are available at https://doi.org/10.1109/TTHZ.2022.3230921.

Digital Object Identifier 10.1109/TTHZ.2022.3230921

(primarily retina and skin), but the technique suffers limitations in terms of penetrability (1.5–2 mm), sensitivity to different compositions, use of a laser as probe, and dimension of the scanned area (around 5 mm) [24], [25], [26]. In these fields, data mined by THz-TDRI would lead to a diagnostic advancement, being the technique able to combine topographic and spectroscopic imaging, without harming the analyzed item.

The spatial phase variation problem has been broadly discussed in literature given the importance of the reflection configuration, and very diverse methodologies have been proposed for phase correction. The majority of these methods have limited application to THz spectroscopy, as the problem is addressed considering the shift in sample position, under the requirement of optically flat object, or using elaborated mathematical approaches or specific instrumental components to remove it [13], [27], [28], [29]. For example, in reflection imaging application, an approach that has been proposed for solving spatial distortion entails the use of laser triangulation system for either precisely adjusting in real-time the distance between THz head and the object, following the shape of the surface, or by conducting multiple planar scans and interpolating them with theoretical model for obtaining virtual scanning surfaces [30]. With both acquisition modes, the time needed to complete the point-to-point correction is long and it requires the use of laser and precise coupling between the two instruments, which is challenging to obtain.

Here we propose a method for tackling the issues generated by the geometrical distortions of the surface that stands out from previously proposed solutions, because it employs a self-referred method that does not need any experimental expedients, such as sophisticated THz devices or the acquisition of multiple measurements. It is based only on the analysis and manipulation of time-domain imaging data, and it is independent of reference signal acquisition. These conditions make the approach flexible and allow the problem generalization. Noteworthy, the same measurements do not force the flattening of the surface sample, such as through a quartz window [31], [32], and this advantageously implies that the approach can be employed also on object that cannot be physically pressed or flattened.

More in details, the proposed method assumes that the global surface distortion individuates a background signal retardation that linearly sum to the temporal shift due to material dispersive properties. The global spatio-temporal distortion of the object is solved by determining the geometrical shape of the surface and removing it as a temporal delay contribution. The adjustment of the temporal profile in time-domain yields to the correction of the electric field phase in the frequency-domain, since the phase linearly shifts with the axial misalignment (see Section III-A). On the contrary, the amplitude of electric field additionally suffers of more complex dependencies on the signal intensity variations along the axial direction, and those magnitude changes cannot be modeled because strictly depend on the dispersive properties of the material.

In the next sections, the individual steps followed to perform the phase correction are described in details, and the limitations of the method performances and conditions for successful experimental results assessed. The benefits of the method are at first demonstrated analyzing a tilted, and highly reflecting surface: a 1 Euro cent coin, scanned horizontal, and then partially tilted for mimicking a not-planar surface with reliefs. The method is then applied on a warped surface, a painting, which represents an object with a variable curvature and with limitations due to absorption. The success of this approach is evaluated against the improvement in the quality of the phase images that are corrupted by imagery artifacts induced by surface distortions.

II. Experimental Setup and Acquisition Procedure

The instrument used in this trial is a commercial THz-TD system (TOPTICA TeraFlash Pro), described in details in a previously published paper [18]. The system is used in reflection configuration, raster-scanning modality, and in a nitrogen-filled environment. The step sizes in both directions were fixed equal to 0.2 mm, and the time trace of a single point was obtained averaging 10 independent measurements.

For each point, the reflected time trace is Fourier transformed to yield the complex field in frequency-domain, expressed in term of phase $\Phi(\omega)$ and amplitude $A(\omega)$

$$\mathcal{F}[E(t)] = \frac{1}{\sqrt{2\pi}} \int_{-\infty}^{+\infty} E(t) e^{-i\omega t} dt = E(\omega) = A(\omega) e^{i\Phi(\omega)}.$$

The frequency resolution of the THz-TD system is given by the time step ($\Delta t = 0.05$ ps) and the number of data points in the time-domain measurement ($N = 1500$), and it is equal to $\Delta\omega = 1/(N\Delta t) = 13$ GHz.

The temporal resolution can be converted into a spatial limit depending on the optical path of the radiation. The equivalent axial resolution can be estimated considering a geometrical approximation of the optical path [13], [33], such as

$$\Delta h = \frac{c}{2\, n_0} \frac{\Delta t}{\cos(\theta)} \tag{1}$$

where c is the light speed, n_0 the refractive index of the medium, θ the incident angle of the radiation, and Δt the temporal distance.

The temporal precision of the instrument was experimentally assessed by measuring the signal peak position from the waveform back reflected from a metallic surface (standard deviation between 5400 scanned points, 10 averages for each position), and it was evaluated to be equal to $\Delta t = 0.15$ ps. Assuming n_0 equal to the unit and the angle of the impinging beam is $\theta = 0.14$ rd, the axial resolution for the object reliefs can be theoretically evaluated to be around $\Delta h = 20$ μm. The lateral resolution is limited by the point spread function (PSF) of the THz beam [34], the dimension of which changes as a function of the frequency ω, and by the acquisition step size along the x and y axis. Assuming a Gaussian beam approximation [34], [35], the beam waist ($2w_0 = 5.094\lambda$) varies between 130 μm and 760 μm, while the Rayleigh length ($z_R = \pi w_0^2/\lambda$) varies between 1 and 6 mm.

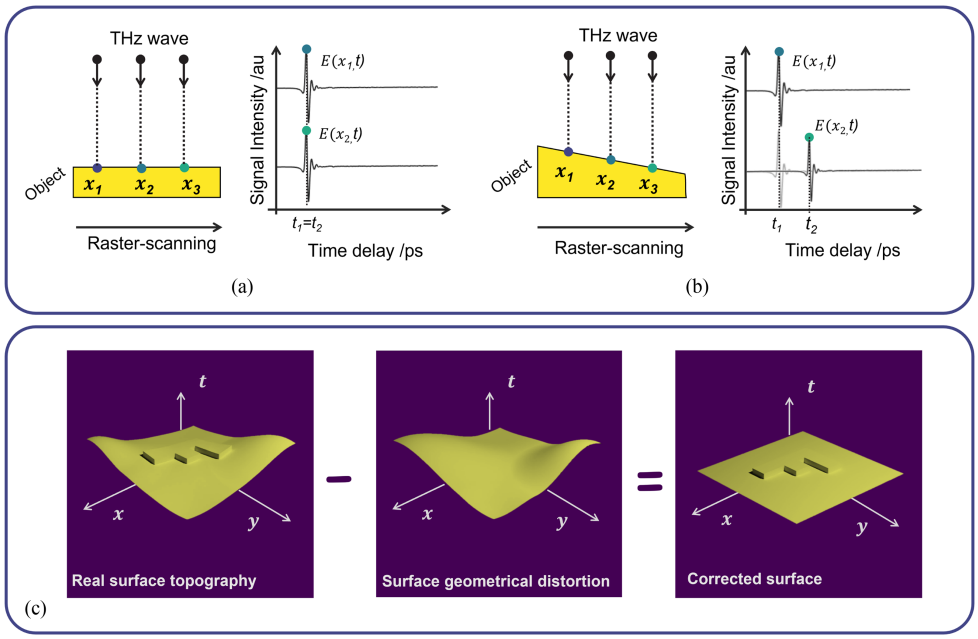

Fig. 1. (a) Left: Raster-scanning measurements made on an ideal object with a flat surface (same height and no morphological defects) and homogeneous material composition; Right: Signals back-reflected from each point of the surface, peaked at $t_1 = t_2 = t_3 = \ldots$, etc., and identical signal features. (b) Left: Raster-scanning measurements made on an object distorted by a surface tilting, but with an uniform composition; Right: Signals delayed and modulated, due to the surface tilt. (c) Example of an object characterised by a surface distortion, owing letter "F" as relief. The figure illustrates the real surface topography as detected by the THz instrument (left), the curve determined by interpolating the surface with a polynomial function (center) and the restored flatness of the surface, without affecting the relief of the object (right).

III. Basic Assumptions for the Correction of the Surface Distortion

A. Problem Statement and Solution

When a THz beam impinges on an ideal object with a flat surface (same height and no morphological defects) and homogeneous material composition [see Fig. 1(a), left], the waves are assumed to be back-reflected from each point with the same temporal delay and with the same signal profile, ignoring the temporal stability of the system. The position of the peak for each signal is at $t_1 = t_2 = t_3 = \ldots$, etc. and the time trace is identical for every point scanned on the object surface [see Fig. 1(a), right]. On the contrary, if the same surface is distorted by a tilting, the reflected space-time pulses is inevitably modified even though the uniformity of the object composition is maintained [see Fig. 1(b), left]. In this case, the peak positions are inevitably shifted of a temporal delay associated to the tilting of the object $t_1 < t_2 < t_3 < \ldots$, etc., and the magnitudes of the time traces are varied accordingly to the out-of-focus alignment [see Fig. 1(b), right]. The exact calculation of the spatio-temporal variation of the field for a tilted object can be extremely complicated, and even more for an irregularly warped surface. In fact, the analytical expressions of the axial variation of the beamlet and the longitudinal intensity profile are represented by composite functions of the frequency components that propagates independently, and of the angular geometrical stretching of the Gaussian beam induced by the object distortion [15].

We assume the problem can be solved in an approximated form, by considering the temporal delay of the THz signal as a linear combination of two components: the shift induced by the dispersive properties of material (τ_n) and the shift generated by the reduced or augmented optical path of the THz radiation due to surface geometrical distortions (τ_g)

$$\tau = \tau_n + \tau_g. \tag{2}$$

The two temporal drift components would be impossible to distinguish if the problem is only locally solved. On the contrary, τ_g can be determined, and thus removed, when it is generated by the global geometry of the object. Under the abovementioned assumptions, τ_g identifies a background signal retardation, associated to the global shape of the object and this contribution can be subtracted by shifting the time traces of the same amount. In this way, the two contributions—the object geometry and the optical response—can be separated, and the surface flatness restored in the time-domain. The general concept of this process is illustrated in Fig. 1(c).

In frequency-domain, the surface distortion modifies both the amplitude and the phase of the electric field, and engenders fictitious imagery artefacts visible in the imaging results. Specifically, Φ carries information on the topography of the object, and the spatio-temporal misalignment of the reflecting surface induces the phase to acquire an additional slope [36], such as

$$\Phi'(\omega) = \Phi(\omega) + \Delta\Phi(\omega, \tau) = \Phi(\omega) + \omega\tau. \tag{3}$$

This implies that the phase is modified by an additive contribution that linearly depends on the frequency, that increases with an increasing misalignment, and that it is higher at higher frequencies. Being a linear problem, the issues generated by surface distortion on $\Phi'(\omega)$ can be repaired adjusting the time

Algorithm 1: Surface Warping Correction.

Input: Ordered THz signals of raster-scanning measurements;
PART 1: Create the three dimensional data (`DataCube`) as series of adjacent scans;
PART 2: Calculate of the highest local maxima of the THz signals along the temporal direction. Define this curve as `ObjSurf`;
PART 3: Interpolate the identified surface and correct the warping:;
(i) Prepare `ObjSurf` and fit data with a polynomial curve (linear or higher degree);
(ii) Calculate the time shift τ_{ij} between interpolated curve and its maximum value;
(iii) Convert τ_{ij} into index steps;
(iv) Create `DataCubeAdj` by shifting `DataCube` of the temporal lag τ_{ij} and employ zero padding at the beginning of the signal;
(v) Calculate $\Phi(\omega)$ and $A(\omega)$ of the electric field in the frequency-domain;
Output: Data cube corrected for surface distortion

trace by the τ_g shift. On the contrary, the amplitude A is affected by the drop of the time trace intensity with respect to the optimized focus position, and by variations that depend on the frequency value, because of the dispersive properties of the material. Overall, the amplitude modifications can be expressed in terms of a modulation contribution

$$A'(\omega) = \chi(\omega, \tau) A(\omega) \tag{4}$$

where $\chi(\omega, \tau)$ is the modulation function that depends on the frequency and the spatio-temporal misalignment. The changes induced on the amplitude cannot be tackled as the $\chi(\omega, \tau)$ is not a simple function of frequency, and of temporal drift, but it depends on the response of the material in the THz frequency region. As an example of that we show how this modulation function affects the amplitude results on a tilted and highly reflective surface.

In the following section, we show how we implemented this method, and how the spatial phase variation problem can be fixed by acting on the temporal drift of the THz signal in time-domain, within specific constraints of applicability.

B. Algorithm

In order to employ the correction described in Section II-I-A, we developed an algorithm to manage and process the data. The algorithm described below is coded in MATLAB (MATLAB R2020b for Window 10, 64 bits) and employs the Curve Fitting Toolbox and the Signal Processing Toolbox [37]. THz time-domain signals compose a three-dimensional matrix, where two dimensions correspond to the raster-scanned surface and the third dimension to the temporal axis of the back-reflected THz signal. The algorithm works on time-domain signals and then calculates the Fourier Transform of the electric field for retrieving the phase $\Phi(\omega)$ and the amplitude $A(\omega)$ in the frequency-domain.

In order to complete the process, the algorithm is structured into three parts, as illustrated in Algorithm 1, and detailed as follows.

PART 1: Creation of the data cube from raster-scanning data. The volume data (`DataCube`) are created by ordering the raster-scanning measurements as a series of adjacent signals along the x and y directions. The `DataCube` is coupled to a vector describing the temporal position.

PART 2: Determination of the peak position. The second part imports the `DataCube` and calculates for each pixel x_{ij} the position of the first peak. This is done by searching for the first highest local maximum of the intensity along the temporal direction, above a certain threshold for the signal intensity. The uncertainty in the identification of the peak positions is mainly determined by the temporal stability of the instrument. The positions of the first peak along the x and y directions are stored in a variable, here named `ObjSurf`, which identifies the maxima isosurface. The `ObjSurf` can be represented as a 3-D curve owning all the roughness features of the object and the temporal uncertainty of the instrument. If the object does not occupy the entire scanned area, the algorithm imposes a threshold for fixing at zero the profiles that does not match the object itself. Afterward, the maxima isosurface is ready for the surface interpolation.

PART 3: Surface interpolation. The third part is the core of the algorithm, and it consists in the interpolation of the surface curvature and its restoration. At this scope, the function *fit* of the Curve Fitting Toolbox of MATLAB is adopted for fitting the data with a polynomial curve based on either linear polynomial surface or higher degree polynomial surface. The result of the interpolation is used to create a surface from the 2-D grid coordinates of the x and y vectors. This polynomial surface is elementwise subtracted to the `ObjSurf` and saved into a matrix named `ObjShape`. For the correction of the surface curvature, the algorithm employed a custom-made function called `SurfaceUnwarping`. This function requires the original `DataCube`, its dimensions, as well as the new `ObjShape` curve as input data. The function `SurfaceUnwarping` generates a matrix whose elements correspond to τ_{ij} values. For every i and j position, τ is taken equal to the temporal distance between the peak position and the peak position at the focus of the beam. Afterward, the `DataCube` signals is shifted accordingly to the τ_{ij} values, and a zero-padding of the same length as the removed temporal trace is added. In this way, the nominal frequency resolution is kept equal to the original THz signal, because the length of the signal is unchanged. Finally, the phase $\Phi(\omega)$ and the amplitude $A(\omega)$ of the electric field are calculated from the adjusted `DataCube` (`DataCubeAdj`) by Fourier transforming the temporal signal (MATLAB function `fft`). The phase is unwrapped accordingly to the method proposed in [38].

In practice, the algorithm can be applied if the sample satisfies three main requirements. First, the surface distortion is smooth compared to local detail variations. In other words, the global variation needs to be larger than the local one. This is because

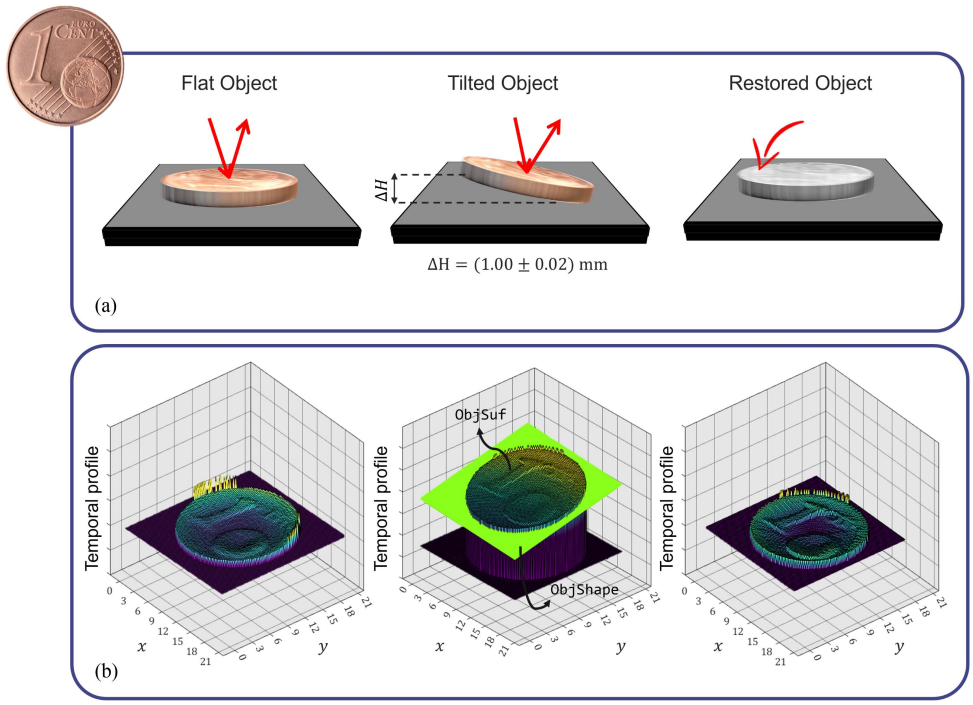

Fig. 2. Picture of the 1 Euro cent coin used for the measurements. (a) Illustrative representation of: (left) object with no curvature positioned horizontal on the motorised stage; (center) object measured with inclination with respect to the horizontal plane (maximum height equal to $\Delta H = 1$ mm); (right) computational correction of the surface tilting. (b) 3-D representation of the isosurface (`ObjSurf`) of the 1 Euro cent coin as flat (left) and tilted (center). The polynomial curve interpolation is indicated as `ObjShape`. On the right, the restored isosurface of the object by employing the proposed method.

the algorithm should be able to separate the two geometries, and employ an interpolation of the surface to remove the global distortion, without damaging local reliefs or valleys. Second, the temporal shift should be smaller than the Rayleigh length of the beam for neglecting the variations induced by the beam dispersion and beam waist, otherwise it would more heavily affect the signal waveform, and consequently the value of the electric field. For our instrument, the maximum temporal shifts τ_{ij} for correcting image distortion up to 3 THz should be lower than 13 ps, corresponding to about 2 mm as axial misalignment (for correcting images at higher frequencies, the maximum time shift reduces accordingly). Third and final requirement relates to the tilting angle. It should not exceed the half of acceptance angle of the collecting parabolic mirror to make valid the condition of negligible signal losses. For our instrument, this requirement imposes a maximum tilting angle of 0.125 rd that corresponds to a max height-gap of 2 mm for an object of 16 mm in size (e.g., coin object). Therefore, the request on the axial misalignment can be considered as conservative as the limitation on the tilting angle in our case.

IV. Experiment

A. Surface Tilting

The self-referenced method is evaluated on a 1 Euro cent coin. The object is made by a copper-covered steel, which is highly reflective in the THz frequency-domain. At first, the acquisition is made by keeping the coin positioned horizontal on the motorized stage of the instrument [see Fig. 2(a), left]. In this case, the object is defined as flat, because it has no specific distortion and the surface is shaped by the reliefs of the coin (stamp of the number one and the globe). The result of the acquisition is used as criterion for comparison with the results obtained after surface tilting correction. In a second stage, the coin is slightly tilted with respect to the horizontal plane [see Fig. 2(a), center]. The lag between the lower and the upper part is estimated about 7.25 ps and, from (1), the inclination height is estimated equal to $\Delta H = 1$ mm. This ΔH value is big enough to induce a phase variation problem, and it can be corrected because it is below the limits of the instrument (details in Section III-B). Finally, the developed algorithm is employed to restore the flatness of the tilted object, as illustrated in Fig. 2(a), right.

The set of τ_{ij} identifies the geometry of the coin when it is posed horizontal on the motorized stage [see Fig. 2(b), left], and the modified surface when the coin is tilted [see Fig. 3(b), center]. Both representations refer to the coin isosurface (`ObjSurf`), as determined in Section III-B. In these examples, a lower threshold is employed for excluding data belonging to the motorized stage that arrives with significant delay with respect to the ones reflected by the object. In order to remove the effect of the spatio-temporal shift, the isosurface of the tilted object is interpolated with a linear polynomial curve (`fitType=poly11`): $Z(x, y) = p_0 + p_1 x + p_2 y$. The result of the fit gives as polynomial coefficients (with 95% confidence bounds): $p_0 = 1.17 \pm 0.01$, $p_1 = (-1.656 \pm 0.030) \cdot 10^{-2}$, and $p_2 = (6.538 \pm 0.003) \cdot 10^{-2}$, and adjusted R-square $= 0.975$. Such a surface is used to correct the curvature of the object with

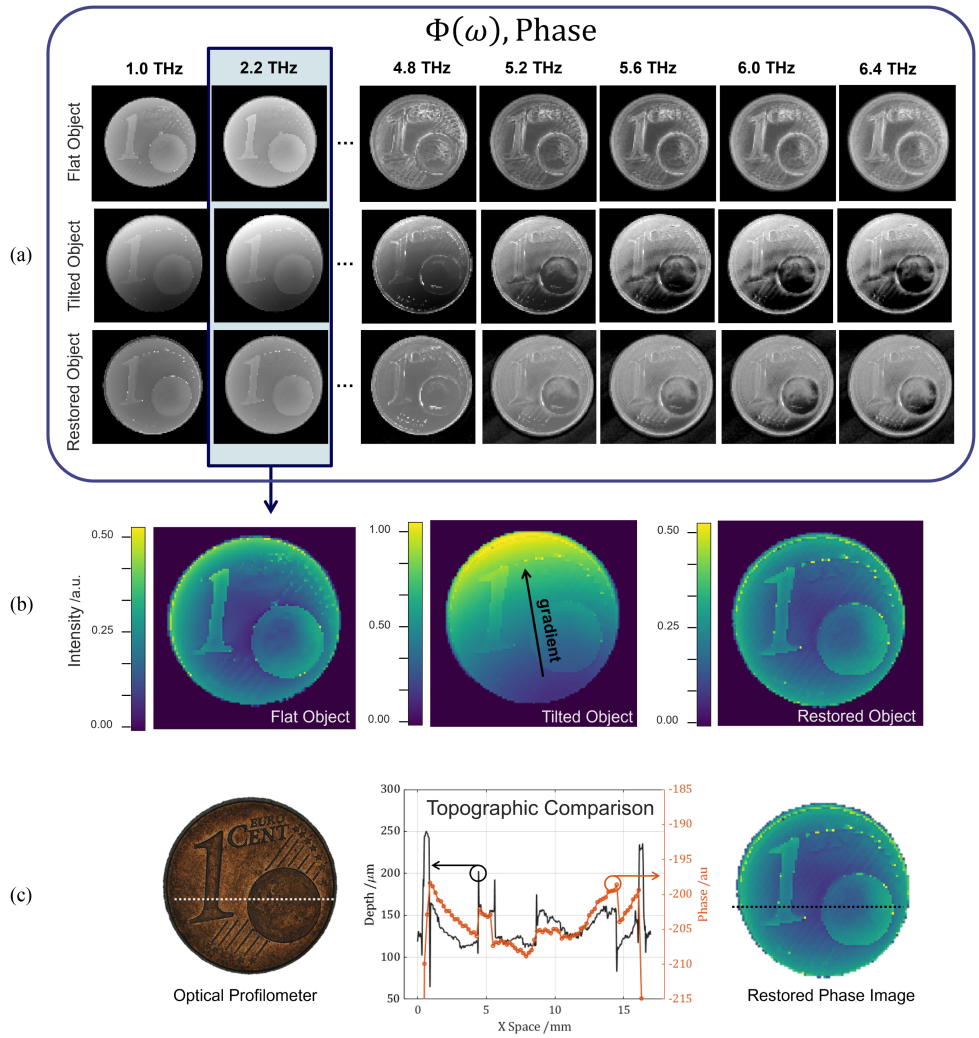

Fig. 3. (a) Results of the $\Phi(\omega)$ at different frequencies. The signal is integrated with $\Delta\omega = 0.4$ THz, in the interval from 1 to 7 THz. Sampling results are presented: flat object (first row), tilted object (second row) and data after surface tilting correction (third row). (b) Detailed comparison between $\Phi(\omega)$ image, integrated in $\omega = 2.2$–2.6 THz, of raw data on flat object, raw data on tilted object, data after surface tilting correction. (c) Comparison of the coin profile acquired with an optical profilometer (Zeta-20, objective M = 10x, NA 0.3) and the phase results of THz-TDRI of the restored surface.

the function `SurfaceUnwarping`, and the `DataCubeAdj` is calculated. The set of τ_{ij} generated by the correction of the temporal signal is shown in Fig. 2(b), right. By Fourier transforming the `DataCubeAdj` from time- to the frequency-domain, the phase $\Phi(\omega)$ and the amplitude $A(\omega)$ are determined.

The phase images for the flat coin object [see first row in Fig. 3(a)] show variations in the gray-scale levels accordingly to the object reliefs. Above 4.8 THz, the signal-to-noise ratio is low, generating images which are slightly corrupted by noise, but still with distinguishable reliefs. In the tilted coin, the phase images are highly affected by the changes in slope of the object at every frequency between 0.2 and 7 THz [see Fig. 3(a), second row]. In particular, they are corrupted by an intensity gradient that goes from the bottom left to the top right side of the object, following the coin inclination. This shade is detectable at low frequencies, and it is further damaged by noise above 5 THz. The intensity gradient is the visual consequence of the additive $\Delta\Phi(\omega)$ and it complicates any type of analyses, especially when they are meant to investigate the surface topography.

The correction of the temporal drift produces the recovery of phase images in the frequency-domain without employing any other data correction, as illustrated in Fig. 3(a), third row. The phase of the `DataCubeAdj` contains contrast features that resembles the ones of the flat object and, more importantly, $\Phi(\omega)$ is corrected for the global distortion of the surface, but the geometries of the reliefs are not modified nor distorted by the computational restoration.

A detailed representation of the consequences on the phase image before and after the computational restoration is reported in Fig. 3(b). Here, the phase results are integrated in the frequencies region $\Delta\omega = 2.2$–2.6 THz, where the signal has good dynamic range. Although the lateral resolution is limited by the instrumental characteristics, the major reliefs in terms of thicknesses (the number one and the globe) are evident on the raw data of the flat object. A concavity in the center of the coin is also distinguishable, while other finer details cannot be revealed with this instrument, because below the lateral resolution of the system. The same shapes appear in the computationally restored object.

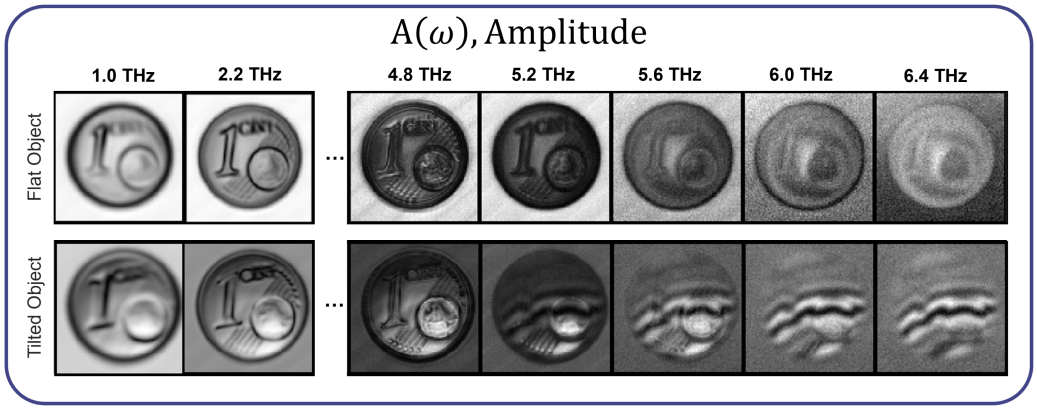

Fig. 4. Explanatory example of the modification induced on the amplitude $A(\omega)$ by surface tilting for different frequencies. The signal is integrated with $\Delta\omega = 0.4$ THz, in the interval from 1 to 7 THz. Sampling results are showed of the flat object (first row), and tilted object (second row).

In order to prove at what extent the developed method can correct the phase, the topographic profile of the coin reconstructed via THz-TDRI is compared with the one obtained from an optical profilometer [see Fig. 3(c)]. The instrument (Profilometer Zeta-20) acquires the optical image of the object at various focal plane and reconstructs the 3-D surface, and it is used to generate quantitative information on the physical roughness and thicknesses. The entire object was scanned stitching together several square acquisitions: the result is displayed in Fig. 3(c), on the left side. The axial resolution of the total image is 1.5 μm. On the right side, Fig. 3(c) displays instead the phase image of the restored phase. Fig. 3(c) represents the line profile of the coin, corresponding to the section running across the number and the globe stamped on the surface for the two acquisitions (optical profilometer and phase reconstruction). This result shows the great similarity of the two profiles, in terms of shapes and reliefs. This comparison not only demonstrated that the evaluation of the object profile can be reliably estimated with THz-TDRI, but also that the correction for surface tilting does not damage these topographic features. The method is robust and capable to restore the shape of distorted surface.

As discussed in Section III-A, the amplitude of the electric field is affected by frequency-dependent modulation of the time trace, and thus its behavior cannot be easily evaluated. For the sake of completeness, we report the results obtained when comparing the amplitude of the flat and tilted coin in Fig. 4. As the amplitude yields information on the reflected intensity of the beam, the results on the coin—made of a highly reflective material at the THz frequencies—are mainly shaped by the object edges when the coin is horizontal. When the object is tilted, the $A(\omega)$ images are corrupted by various artifacts. In the frequency region with good dynamic range (0.1–3.5 THz), the amplitude images suffer of greater blurring effects, and of slight intensity gradient along the inclination of the coin, with respect to the flat example. At high frequency, the $A(\omega)$ images are damaged by wavy features, detected at fixed frequency and different axial misalignment. Such an intensity modulation has a small contribution (0.1 dB), and thus it appears only when the amplitude signal reaches the noise floor. This is one of the consequences of the distortion of the signal waveform that shows up on the electric field amplitude in the frequency-domain.

B. Surface Warping

The self-referenced method enables the removal of irregular surface distortion, as long as the surface curvature can be fitted with a polynomial function and the conditions described in Section III-B are valid. While the choice of the polynomial order is still a manual input parameter at present, we show here that even for a realistic and complex example, a relatively low-order polynomial can be accurate enough to solve phase variation problem. In this Section, the algorithm is applied on a warped surface, a painting on wood canvas, in order to demonstrate the applicability of the method when more complex distortions are present. The considered painting is an object that has irregularities due to the overlapping of multiple pictorial layers (as reported in [39]), heterogeneous pictorial composition (with different refractive index), and distortions at micrometer scale, as revealed by the time traces. To draw a parallel with the object analyzed above, the brush strokes act as the object reliefs and depressions, while the curvature of the wood support determines the surface distortion of the object. The analysis of the time traces reveals that the lag between the minimum and the maximum value of τ is 12.65 ps, thus near the limit imposed by the instrument for an adequate correction of the surface distortion up to 3 THz.

Fig. 5(a) shows the painting used in the test, depicting a face of a lady as subject. A portion of the painting was scanned (area of 70×65 mm^2) and the results in time-domain are displayed in Fig. 5(b). The 3-D representation of the peak position of the time traces showed a highly irregular surface, e.g., the signals from the lady's forehead are highly misaligned with respect to the ones from the overall surface [see Fig. 5(b), left]. On the contrary to the case of the tilted object, here the surface was interpolated with a higher degree of polynomial curve (MATLAB function `poly23`), corresponding to a second-order polynomial in the x and a third-order polynomial in the y direction. The result of the interpolating process is showed in Fig. 5(b), center. In time-domain, the subtraction of the curve to the surface geometry allowed to eliminate the issue generated by distortion of the wood support and maintain the reliefs, concavities, and irregularities of the pictorial surface [see Fig. 5(b), right]. This example on an heterogeneous object demonstrates that the assumption of the

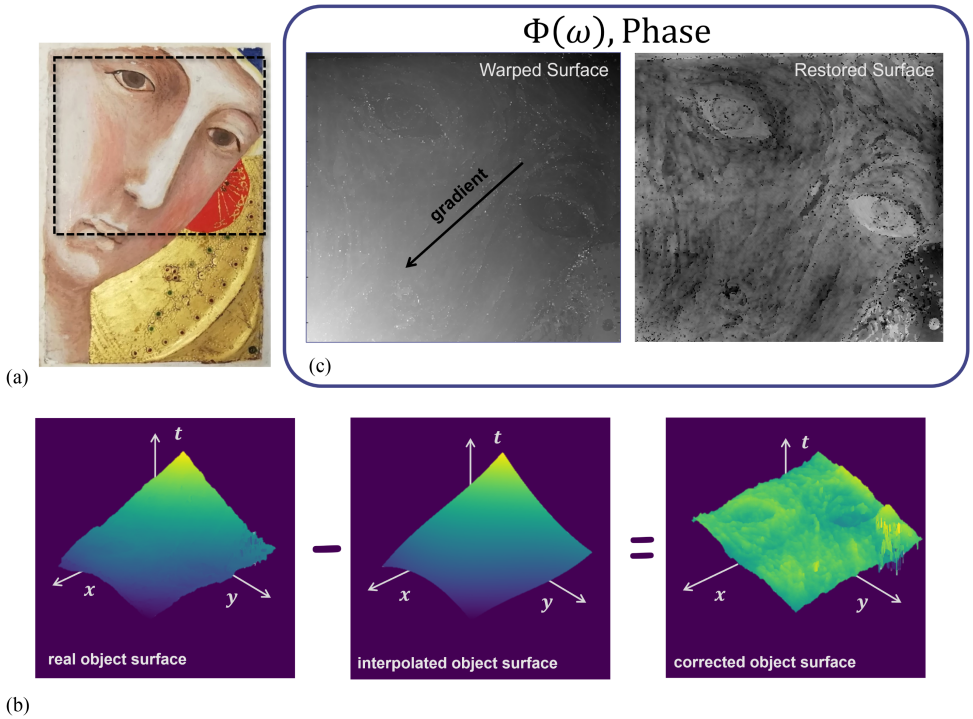

Fig. 5. (a) Picture of the painting made on wood support employed as an example of warped surface. (b) On the left: the representation of the surface topography (`ObjSurf`), on the center the curve determined by interpolating the surface with a polynomial function (`ObjShape`) and on the right, the restored flatness of the painting in time-domain. (c) Comparison between $\Phi(\omega)$ image, integrated in $\omega = 2.2$–2.6 THz, of raw data and data after surface curvature correction.

linear contribution of τ_g to the temporal drift can be considered a good approximation for the phase correction. In details, Fig. 5(c) shows the phase results obtained before and after correction for the geometrical curvature of the surface (signal integrated over a range $\Delta\omega$ =2.0–2.4 THz). On the warped surface, the phase intensity is corrupted by an intensity gradient ($\Delta\Phi$) associated to the warping of the surface, and superimposed to the topography of the painting. In the same frequency region, the intensities of the phase after the surface correction make evident the distribution of heterogeneous materials with different dispersive properties, corresponding to lighter or darker gray pixels in the phase images. As for the case of the tilted surface, the warping correction does not cause any evident imagery artifacts, although a flat replica of this object is not available. On this example, the contribution to the phase slope after time trace correction, is only assigned to the response of the materials in the THz frequencies and thus can be reliably used for further spectroscopic analysis.

V. Conclusion

The surface physical distortions of an object can strongly limit the analysis of THz-TDRI results, as it produces phase variation and fictitious artifacts in the imagery representation of the electric field in the frequency-domain. We proposed a self-referenced method capable to solve the spatial phase variation problem by assuming that the temporal drift associated to the geometrical distortions linearly contributes to the shift of the THz time trace. We demonstrated the benefits of such approach on a tilted and highly reflective surface, and a warped and heterogeneous surface.

We showed that the phase of the signal can be retrieved by correcting the signal retardation in time-domain. The limitations of the method rely in the accuracy of the interpolation of the physical surface distortion and in the maximum temporal drift acceptable. For example, the latter was estimated equal to 13 ps for the system PSF, corresponding to about 2 mm in height. Apart from not requiring any numerical parameter optimization, the advantage of the proposed approach is that the method adjusts the global warping by acting on the temporal shift of the electric field in time-domain data and this prevents from the corruption of the spectral signature in frequency domain of the phase value. By adopting this preprocessing tool, the response of the object in the THz region can be reliably retrieved also on curved surfaces, when THz-TDS is used in reflection geometry and the surface distortion cannot be removed.

Acknowledgment

The authors would like to thank Dr. Marco Salerno (Materials Characterization Facility, Istituto Italiano di Tecnologia) for the support with the Optical Profilometer.

References

[1] J. Neu and C. A. Schmuttenmaer, "Tutorial: An introduction to terahertz time domain spectroscopy (THZ-TDS)," *J. Appl. Phys.*, vol. 124, no. 23, 2018, Art. no. 231101. [Online]. Available: https://doi.org/10.1063/1.5047659

[2] S. Wietzke et al., "Terahertz spectroscopy: A powerful tool for the characterization of plastic materials," in *Proc. IEEE 10th Int. Conf. Solid Dielectrics*, 2010, pp. 1–4.

[3] S. Wietzke et al., "Terahertz spectroscopy on polymers: A review of morphological studies," *J. Mol. Struct.*, vol. 1006, no. 1, pp. 41–51, 2011. [Online]. Available: https://www.sciencedirect.com/science/article/pii/S002228601100593X

[4] J. Savolainen, S. Ahmed, and P. Hamm, "Two-dimensional Raman-terahertz spectroscopy of water," *Proc. Nat. Acad. Sci.*, vol. 110, no. 51, pp. 20402–20407, 2013. [Online]. Available: https://www.pnas.org/content/110/51/20402

[5] Z. Wang et al., "Characterization of thin metal films using terahertz spectroscopy," *IEEE Trans. THz Sci. Technol.*, vol. 8, no. 2, pp. 161–164, Mar. 2018.

[6] M. M. Nazarov, A. P. Shkurinov, E. A. Kuleshov, and V. V. Tuchin, "Terahertz time-domain spectroscopy of biological tissues," *Quantum Electron.*, vol. 38, no. 7, pp. 647–654, Jul. 2008. [Online]. Available: https://doi.org/10.1070/qe2008v038n07abeh013851

[7] L. Afsah-Hejri et al., "Terahertz spectroscopy and imaging: A review on agricultural applications," *Comput. Electron. Agriculture*, vol. 177, 2020, Art. no. 105628. [Online]. Available: https://www.sciencedirect.com/science/article/pii/S0168169919318204

[8] N. B. Lawler, D. Ho, C. W. Evans, V. P. Wallace, and K. S. Iyer, "Convergence of terahertz radiation and nanotechnology," *J. Mater. Chem. C*, vol. 8, pp. 10942–10955, 2020. [Online]. Available: http://dx.doi.org/10.1039/D0TC01716 G

[9] M. Naftaly, N. Vieweg, and A. Deninger, "Industrial applications of terahertz sensing: State of play," *Sensors*, vol. 19, no. 19, 2019, Art. no. 4203. [Online]. Available: https://www.mdpi.com/1424-8220/19/19/4203

[10] H. Guerboukha, K. Nallappan, and M. Skorobogatiy, "Toward real-time terahertz imaging," *Adv. Opt. Photon.*, vol. 10, no. 4, pp. 843–938, Dec. 2018. [Online]. Available: http://aop.osa.org/abstract.cfm?URI=aop-10-4-843

[11] B. Ferguson and X.-C. Zhang, "Materials for terahertz science and technology," *Nature Mater.*, vol. 1, no. 1, pp. 26–33, 2002. [Online]. Available: https://doi.org/10.1038/nmat708

[12] J. El Haddad, B. Bousquet, L. Canioni, and P. Mounaix, "Review in terahertz spectral analysis," *TrAC Trends Anal. Chem.*, vol. 44, pp. 98–105, 2013. [Online]. Available: https://www.sciencedirect.com/science/article/pii/S0165993613000022

[13] A. Pashkin, M. Kempa, H. Němec, F. Kadlec, and P. Kužel, "Phase-sensitive time-domain terahertz reflection spectroscopy," *Rev. Sci. Instruments*, vol. 74, no. 11, pp. 4711–4717, 2003. [Online]. Available: https://doi.org/10.1063/1.1614878

[14] X. Gu, S. Akturk, and R. Trebino, "Spatial chirp in ultrafast optics," *Opt. Commun.*, vol. 242, no. 4, pp. 599–604, 2004. [Online]. Available: https://www.sciencedirect.com/science/article/pii/S0030401804008855

[15] C. G. Durfee, M. Greco, E. Block, D. Vitek, and J. A. Squier, "Intuitive analysis of space-time focusing with double-abcd calculation," *Opt. Exp.*, vol. 20, no. 13, pp. 14244–14259, Jun. 2012. [Online]. Available: http://www.osapublishing.org/oe/abstract.cfm?URI=oe-20-13-14244

[16] M. Picollo, K. Fukunaga, and J. Labaune, "Obtaining noninvasive stratigraphic details of panel paintings using terahertz time domain spectroscopy imaging system," *J. Cultural Heritage*, vol. 16, no. 1, pp. 73–80, 2015. [Online]. Available: https://www.sciencedirect.com/science/article/pii/S1296207414000193

[17] K. Krügener et al., "Terahertz inspection of buildings and architectural art," *Appl. Sci.*, vol. 10, no. 15, 2020, Art. no. 5166. [Online]. Available: https://www.mdpi.com/2076-3417/10/15/5166

[18] A. Artesani, R. Lamuraglia, F. Menegazzo, S. Bonetti, and A. Traviglia, "Terahertz time-domain spectroscopy in reflection configuration for inorganic and mineral pigment identification," *Appl. Spectrosc.*, to be published, doi: 10.1177/00037028221133404.

[19] A. I. McIntosh, B. Yang, S. M. Goldup, M. Watkinson, and R. S. Donnan, "Terahertz spectroscopy: A powerful new tool for the chemical sciences?," *Chem. Soc. Rev.*, vol. 41, pp. 2072–2082, 2012. [Online]. Available: http://dx.doi.org/10.1039/C1CS15277 G

[20] X. Yang et al., "Biomedical applications of terahertz spectroscopy and imaging," *Trends Biotechnol.*, vol. 34, no. 10, pp. 810–824, 2016. [Online]. Available: https://www.sciencedirect.com/science/article/pii/S0167779916300270

[21] C. Seco-Martorell et al., "Goya's artwork imaging with terahertz waves," *Opt. Exp.*, vol. 21, no. 15, pp. 17800–17805, Jul., 2013. [Online]. Available: http://www.opticsexpress.org/abstract.cfm?URI=oe-21-15-17800

[22] M.-A. Brun et al., "Terahertz imaging applied to cancer diagnosis," *Phys. Med. Biol.*, vol. 55, no. 16, pp. 4615–4623, Jul. 2010. [Online]. Available: https://doi.org/10.1088/0031-9155/55/16/001

[23] Y. Peng, C. Shi, X. Wu, Y. Zhu, and S. Zhuang, "Terahertz imaging and spectroscopy in cancer diagnostics: A technical review," *BME Front.*, vol. 2020, pp. 1–11, 2020.

[24] H. Liang et al., "Optical coherence tomography and non-linear microscopy for paintings–a study of the complementary capabilities and laser degradation effects," *Opt. Exp.*, vol. 25, no. 16, pp. 19640–19653, Aug. 2017. [Online]. Available: http://www.opticsexpress.org/abstract.cfm?URI=oe-25-16-19640

[25] A. P. Wax, "Seeing deep into engineered samples with dual-axis OCT," in *Proc. Opt. Methods Inspection, Characterization, Imag. Biomaterials*, 2021, Art. no. 1178603. [Online]. Available: https://doi.org/10.1117/12.2593463

[26] C. L. K. Dandolo et al., "Toward a multimodal fusion of layered cultural object images: Complementarity of optical coherence tomography and terahertz time-domain imaging in the heritage field," *Appl. Opt.*, vol. 58, no. 5, pp. 1281–1290, Feb. 2019. [Online]. Available: http://ao.osa.org/abstract.cfm?URI=ao-58-5-1281

[27] T. Nagashima and M. Hangyo, "Measurement of complex optical constants of a highly doped SI wafer using terahertz ellipsometry," *Appl. Phys. Lett.*, vol. 79, no. 24, pp. 3917–3919, 2001. [Online]. Available: https://doi.org/10.1063/1.1426258

[28] D. Hashimshony et al., "Characterization of the electrical properties and thickness of thin epitaxial semiconductor layers by THz reflection spectroscopy," *J. Appl. Phys.*, vol. 90, no. 11, pp. 5778–5781, 2001. [Online]. Available: https://doi.org/10.1063/1.1412574

[29] E. M. Vartiainen et al., "Numerical phase correction method for terahertz time-domain reflection spectroscopy," *J. Appl. Phys.*, vol. 96, no. 8, pp. 4171–4175, 2004. [Online]. Available: https://doi.org/10.1063/1.1786345

[30] A. Doria et al., "An alternative phase-sensitive THz imaging technique for art conservation: History and new developments at the ENEA center of frascati," *Appl. Sci.*, vol. 10, no. 21, 2020, Art. no. 7661. [Online]. Available: https://www.mdpi.com/2076-3417/10/21/7661

[31] S. Fan, E. P. J. Parrott, B. S. Y. Ung, and E. Pickwell-MacPherson, "Calibration method to improve the accuracy of THz imaging and spectroscopy in reflection geometry," *Photon. Res.*, vol. 4, no. 3, pp. A29–A35, Jun. 2016. [Online]. Available: https://opg.optica.org/prj/abstract.cfm?URI=prj-4-3-A29

[32] S. Huang et al., "Improved sample characterization in terahertz reflection imaging and spectroscopy," *Opt. Exp.*, vol. 17, no. 5, pp. 3848–3854, Mar. 2009. [Online]. Available: https://opg.optica.org/oe/abstract.cfm?URI=oe-17-5-3848

[33] F. Vandrevala and E. Einarsson, "Decoupling substrate thickness and refractive index measurement in THz time-domain spectroscopy," *Opt. Exp.*, vol. 26, no. 2, pp. 1697–1702, Jan. 2018. [Online]. Available: http://www.opticsexpress.org/abstract.cfm?URI=oe-26-2-1697

[34] M. Ljubenović, A. Artesani, S. Bonetti, and A. Traviglia, "Beam-shape effects and noise removal from THz time-domain images in reflection geometry in the 0.25-6 THz range," *IEEE Trans. THz Sci. Technol.*, vol. 12, no. 6, pp. 574–586, 2022, doi: 10.1109/TTHZ.2022.3196191.

[35] B. Recur et al., "Propagation beam consideration for 3D THz computed tomography," *Opt. Exp.*, vol. 20, no. 6, pp. 5817–5829, Mar. 2012. [Online]. Available: http://www.opticsexpress.org/abstract.cfm?URI=oe-20-6-5817

[36] S. Watanabe, "Terahertz polarization imaging and its applications," *Photonics*, vol. 5, no. 4, 2018, Art. no. 58. [Online]. Available: https://www.mdpi.com/2304-6732/5/4/58

[37] *MATLAB, R 2021 b Update 2*. Natick, MA, USA: The MathWorks Inc., 2022.

[38] P. U. Jepsen, "Phase retrieval in terahertz time-domain measurements: A 'how to' tutorial," *J. Infrared, Millimeter, Terahertz Waves*, vol. 40, no. 4, pp. 395–411, 2019. [Online]. Available: https://doi.org/10.1007/s10762-019-00578-0

[39] S. Mosca et al., "A whole spectroscopic mapping approach for studying the spatial distribution of pigments in paintings," *Appl. Phys. A*, vol. 122, no. 9, pp. 1–10, 2016. [Online]. Available: https://doi.org/10.1007/s00339-016-0345-8

Open Access provided by 'Istituto Italiano di Tecnologia' within the CRUI CARE Agreement